

A Novel Perspective of a Laguerre–Gaussian Beam’s Phase Acceleration in Chiral Medium by Using Distinguishability Property

Francisco E. Alban-Chacón , Arturo Pazmiño , Peter Iza , Manuel S. Alvarez-Alvarado , and Erick A. Lamilla-Rubio

Abstract—The concept of orbital angular momentum has gained significant interest in recent years across various fields of science, particularly in physics and biology. In this article, we present a novel approach to investigating the acceleration and deceleration of the phase distribution of a Laguerre–Gaussian beam. Our model proposes a topological transformation from a canonical vortex to a non-canonical vortex when the beam interacts with a chiral medium, based on a generalized distinguishability property of the vortex. We compare our model’s predictions with phase acceleration data from simulations by Liu et al., showing excellent agreement. Additionally, we provide a quantum mechanical interpretation of our model. Our results show that the elliptical beam resulting from passing through a slab of chiral media is a superposition of various LG modes of the topological charge l . We conclude that the distinguishability property of a canonical vortex beam, where $\omega \propto \frac{1}{l}$, holds physical significance and practical relevance.

Index Terms—Chiral medium, LG beam, non-canonical vortex, OAM, phase acceleration.

I. INTRODUCTION

ORBITAL angular momentum of light has become a milestone for many applications in different fields such as optical communications by increasing the capacity of data transmission using spatial multiplexing [1], [2], [3], [4], and also improving the information coding [5], [6], [7], [8], [9], [10]; image processing by improving imaging resolution [11], [12]; particle manipulation using optical tweezers [13], [14], [15]; and so on.

Light beams carrying orbital angular momentum has a helical structure in its wavefront and phase distribution that depends on $\exp(-il\phi)$, in which ϕ is the azimuthal coordinate of the beam’s cross section, and l is the topological charge (or azimuthal index) that can take integer and fractional values [16], [17], [18].

Manuscript received 8 June 2023; revised 29 July 2023; accepted 15 August 2023. Date of publication 17 August 2023; date of current version 29 August 2023. (Corresponding author: Francisco E. Alban-Chacón.)

Francisco E. Alban-Chacón, Arturo Pazmiño, and Erick A. Lamilla-Rubio are with the Escuela Superior Politécnica del Litoral, ESPOL, Facultad de Ciencias Naturales y Matemáticas, Guayaquil 09-01-5863, Ecuador (e-mail: alban@espol.edu.ec).

Peter Iza is with the Escuela Superior Politécnica del Litoral, ESPOL, Facultad de Ciencias Naturales y Matemáticas, Guayaquil 09-01-5863, Ecuador, and also with the Center of Research and Development in Nanotechnology, CIDNA, Escuela Superior Politécnica del Litoral, ESPOL, Guayaquil 09-01-5863, Ecuador.

Manuel S. Alvarez-Alvarado is with the Escuela Superior Politécnica del Litoral, ESPOL, Facultad de Ingeniería Eléctrica y Computación (FIEC), Guayaquil 09-01-5863, Ecuador.

Digital Object Identifier 10.1109/JPHOT.2023.3306162

An optical beam propagating in the $-z$ -direction in free space can be expressed as: $E(r, \phi, z) = U(r, \phi, z) \exp(-ikz)$, where $U(r, \phi, z)$ is the amplitude of the beam in cylindrical coordinates, and the cylindrically symmetric solution for a LG beam is given by [19], [20]. The phase distribution associated to this LG beam is:

$$\Phi(r, z, \omega) = kz + \frac{kr^2}{2R_z} + l\phi - (2p + |l| + 1) \tan^{-1} \frac{z}{z_0} \quad (1)$$

where $k = 2\pi/\lambda$ is the wave number, $R_z = z(1 + (z_0/z)^2)$ is the radius of curvature, and $z_0 = (\pi w_0^2)/\lambda$ is the Rayleigh range. The term $\tan^{-1}(z/z_0)$ is the Gouy’s phase multiplied by the mode order $(2p + |l| + 1)$ that contains the radial index p and the topological charge index l of a LG vortex beam.

Previous experiments and simulations had recently been conducted to study the dynamics of an off beam dielectric particle (with diameter $\ll \lambda$) interacting with a LG beam [21], [22], [23]. These studies were motivated by its application to biology, in which LG beams can be used as optical tweezers, optical spanners or optical screwdrivers [24].

Liu et al. [23] reported that in a chiral medium a linearly polarized LG beam phase suffers an acceleration and deceleration in two regions of space to along the beam direction z . Constants parameters were chosen so that k or ν_0 do not change (i.e., linear momentum per photon is constant). Constitutive equations in the Tellegen form [25] are used to model the chiral medium. The chiral parameter chosen by Liu is $\kappa = 0.05$ (nondispersive and lossless medium that is not difficult to obtain experimentally). Then, a LG beam is interacting with this chiral medium. From this mathematical model, the evolution of the phase distribution vs propagation distance is plotted, and regions where this phase accelerates and decelerates are analyzed. It is then concluded that regions of phase acceleration and deceleration are important since torque is enhanced.

In this work, a novel perspective for analyzing the phase acceleration of an LG beam in a chiral medium, using a non-canonical vortex mathematical model and the distinguishability property for the topological charge, is presented. The physical origin of this phase acceleration seems to be unknown/unexplained and there relies the relevance of this article. Further, from the application point of view this article is important since we attempt to provide and initiate a new analytical way of associating properties of extrema of derivatives of phase speed with extrema

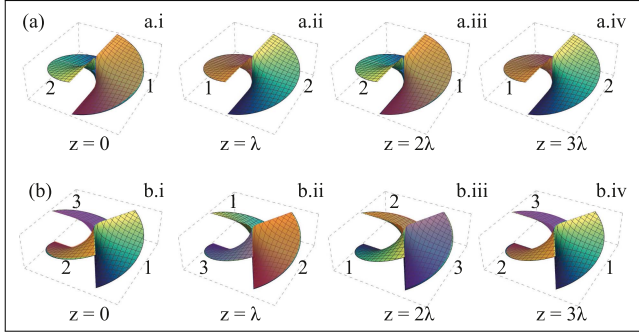


Fig. 1. Rotation of the Laguerre–Gaussian phase distribution beam is tracked for (a) $l = 2$ and (b) $l = 3$, using a beam waist $\omega_0 = 5.0$ mm and wavelength $\lambda = 700$ nm at different points along the axis propagation, i. $z = 0$, ii. $z = \lambda$, iii. $z = 2\lambda$, iv. $z = 3\lambda$.

of torque when placing a probe particle in a chiral medium. It is hoped this could be used in physical and biological experiments (i.e.; optical tweezers).

A. Distinguishability Property

The phase distribution of a vortex beam rotates along the optical axis as the light beam moves through free space. Using simulations of the Laguerre–Gaussian equation is possible to show that this rotation depends on the azimuthal index l by tracking the phase distribution at different points along the propagation axis. The main results can be found in detail in [20]. In summary, Fig. 1 shows the simulation of the phase distribution of a LG beam with a beam waist $\omega_0 = 5.0$ mm and wavelength $\lambda = 700$ nm for two different values of the topological charge l . Fig. 1(a) shows the tracking rotation of the phase distribution for a LG beam when $l = 2$. The reference phase distribution is taken at $z = 0$ (Fig. 1(a.i)), then at $z = \lambda$ the distribution had a half rotation (Fig. 1(a.ii)), a full rotation at $z = 2\lambda$ (Fig. 1(a.iii)), and another half rotation at $z = 3\lambda$ (Fig. 1(a.iv)). Fig. 1(b) shows the tracking rotation of the phase distribution for a LG beam when $l = 3$. Again, the reference phase distribution is taken at $z = 0$ (Fig. 1(b.i)), then at $z = \lambda$ the distribution had a rotation of $2\pi/l$, i.e. 120 degrees (Fig. 1(b.ii)), at $z = 2\lambda$ the distribution had rotated $4\pi/l$, i.e. 240 degrees (Fig. 1(b.iii)), and a full rotation at $z = 3\lambda$ (Fig. 1(b.iv)).

The main results from simulating the LG beam equation are that the rotational speed depends only on the topological index parameter l , the radial index p does not affect this speed. The more helices in the phase distribution, given by the parameter l , the slower the rotational speed for the phase distribution, rising a distinguishability characteristic [20]:

$$\omega = \frac{k\nu_0}{l} \quad (2)$$

where ν_0 is the propagation velocity of the vortex beam along the z axis.

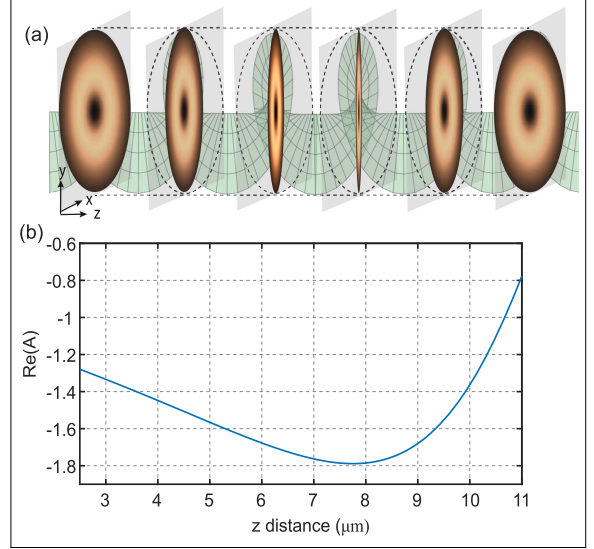


Fig. 2. (a) Evolution of a non-canonical elliptical vortex inside a chiral medium during its propagation. (b) The real part of the non-canonical strength, $Re(A)$, vs z graph. As the $Re(A)$ decreases the eccentricity of the elliptical vortex in (a) increases up till the minima then the $Re(A)$ increases again and the eccentricity in (a) decreases. The location of the minima in this Fig. depends on the chirality κ .

B. Non-canonical Optical Vortex Model of an LG Beam in a Chiral Medium

When a linearly polarized beam of light interacts with chiral medium, circular dichroism occurs [26], [27]. Then, if an incoming linearly polarized LG beam is passing through a chiral medium the radial symmetry of the beam is broken, and one can treat the beam as a single elliptical beam that encloses a non-canonical vortex [28], [29] (see Fig. 2(a)). The effective beam can be approximately modelled with an elliptical Gaussian beam envelope covering a non-canonical vortex [30] (i.e. is not singular, but has a geometry and evolves continuously in z). As an important clarification, although LG beams with different topological charge are shown in Fig. 1, this is for illustrative purposes. The case of an incoming $l = 1$ LG beam is analyzed in this article without loss of generality. This is since any higher order of topological charge would be unstable against asymmetric deformation, breaking apart into their single charge components [28], [29]. Further, for $l = -1$ it could be observed that the results obtained in this article will show no physically meaningful difference. Now, Fig. 2(b)) shows the evolution of the real part of the non-canonical strength of the vortex, to qualitatively explain the change in the ellipse eccentricity.

The strength of this vortex is measured by A [28] and a natural interpretation of $Re(A)$ is that it is a measure of the twisting of the vortex. (i.e. it can be seen as a function of the strength of the vorticity and to be proportional to local angular momentum of the non-canonical vortex). For an elliptical Gaussian beam a non-canonical vortex strength A is a complex number and evolves in z as [29]:

$$A(z) = A_0(\lambda, \kappa) \frac{2(z - z_x) - iw_{0x}^2}{2(z - z_y) - iw_{0y}^2} \quad (3)$$

Here z_x, z_y are the location of the beam waists along the propagation axis, w_{0x} and w_{0y} are the beam waist in the plane xy , and $A_0(\lambda, \kappa)$ is a constant that depends on the initial conditions, and therefore, it must be a function of the wavelength of the beam λ and the chirality parameter κ of the medium. The real part of A can be seen as a natural generalization of the singular topological charge l of the vortex [29]. The sign of $Re(A)$ indicates the sign of this topological charge. Further, a change of the sign of the topological charge, e.g. $l = -1$, shows no physically meaningful difference in the results obtained in this article.

Now, using the distinguishability property discussed in [20] and summarized in this letter, a natural generalization of the theory above for a non-canonical vortex to calculate its phase speed of rotation, ω_{non} , can be expressed as:

$$\omega_{non} = \frac{k\nu_0}{Re(A)} \quad (4)$$

Where $Re(A)$ is a function of the real part of the strength of the non-canonical vortex, the wave number $k = \frac{2\pi}{\lambda}$, with λ being the physical wavelength of the beam and ν_0 is the linear speed of propagation of the phase. To investigate the validity of (4) is useful to write it in another form. The general equation of the linear phase speed of propagation of a wave is:

$$\nu_0 = \lambda_{ph} f \quad (5)$$

Where λ_{ph} is the wavelength of the wave in a chiral medium, and f is the phase rotation frequency (i.e. note that $\omega_{non} = 2\pi f$). Comparing (5) and (4) one obtains:

$$\lambda_{ph} = Re(A)\lambda \quad (6)$$

Therefore, from previous equation, when $Re(A)$ changes along z the wavelength of the wave in a chiral medium also varies. Now, the derivative with respect to z is taken to the equation above, since it provides a more suitable form of the equation to compare with the appropriate data. This can be interpreted through the following equation:

$$\frac{\frac{d\lambda_{ph}}{dz}}{\lambda} = \frac{dRe(A)}{dz} \quad (7)$$

II. APPLICATION AND RESULTS

With the intention of verifying the validity of equation 4, the data from [23], of phase vs z in their graph of Fig. 1(a), was used at regular intervals of $\Delta z \sim 0.1 \mu\text{m}$ (for clarity purposes a similar figure is reproduced here that illustrates the same trend in phase vs z in Fig. 3(b)). The relative difference with respect to z , in wavelength, between the two curves is calculated (i.e. chiral medium with $\kappa = 0.05$ and reference curve, achiral case, see Fig. 3(b)). Then, this is divided by $\lambda = 700 \text{ nm}$, and a polynomial fit is performed. Finally, this is plotted against z (depicted in Fig. 3(a) as “Tellegen model”) for the interval $z = 0 \mu\text{m}$ to $12 \mu\text{m}$. This corresponds to the left hand side of (7). The right hand side was derived from (3) by using parameters from [23], such as $z_x = z_y = 12 \mu\text{m}$ and $w_{0x} = 1 \mu\text{m}$. The values of A_0 and w_{0y} were adjusted empirically as the best free parameter that can model the data from [23], obtaining $A_0 = 0.25 - 4.3i$ and $w_{0y} = 3 \mu\text{m}$. The curve is depicted in Fig. 3(a) as “non

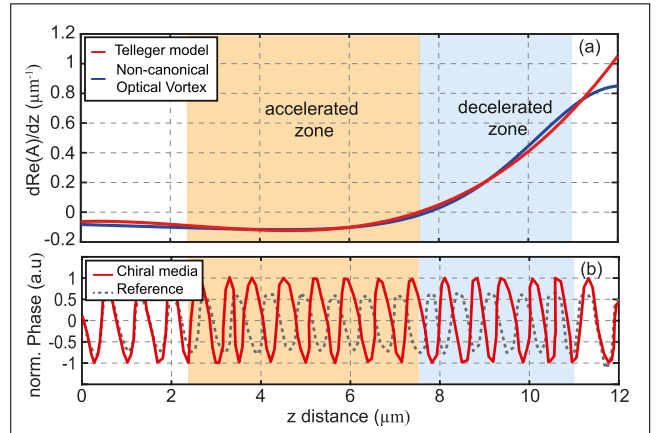


Fig. 3. Comparison between the Tellegen model and the non-canonical optical vortex model. (a) The red solid curve was obtained by fitting a cubic polynomial to the data obtained in [23] (in which the Tellegen model was used). The blue solid curve is obtained by using the non-canonical optical vortex model. (b) This graph illustrates the trend of the phase vs z of a LG beam used in [23] in a chiral and achiral cases. The red solid curve is for $\kappa = 0.05$ (chiral case) and the blue dashed curve is used as a reference (achiral case).

canonical optical vortex model”. These results are presented in Fig. 3, having excellent agreement. $A_0 = 0.25 - 4.3i$ and $w_{0y} = 3 \mu\text{m}$. The curve is depicted in Fig. 3(a) as “non canonical optical vortex model”. These results are presented in Fig. 3, having excellent agreement.

It can be seen from Fig. 3(a) that the two models predict similar behavior, validating (7), and more importantly (4). Further, the normalized root mean squared error between $2.5 \mu\text{m}$ up till $11.5 \mu\text{m}$ approx is found to be 0.37, which indicates the model approximation proposed here can explain accurately the data in this region. Note that at the region up till $2.5 \mu\text{m}$ there is no perceptible phase acceleration, reported in [23], and therefore the model, for the red solid curve, proposed here cannot capture such data.

Also, in Fig. 3(b) there are two waves. One is used as reference (achiral medium). The other one, corresponds to the chiral medium case and it can be seen that the frequency of the wave (i.e. phase) is incremented (this means there is a phase acceleration) starting at $2.5 \mu\text{m}$, this goes up till around $7.8 \mu\text{m}$ (accelerated region). The location of this endpoint depends on the chirality κ of the medium). Then, the frequency decreases (phase deceleration) and the two curves coincide again up till $11.5 \mu\text{m}$ (decelerated region).

Furthermore, from the behaviour of the real part of the non-canonical strength, $Re(A)$, in Fig. 2(b), it can be inferred that the acceleration and deceleration is related the slope of this graph. Negative slope means an acceleration of the LG vortex phase speed, and a positive slope is a deceleration of this phase speed. Moreover, it can be interpreted that the steeper the slope, the faster the phase speed accelerates/decelerates. Then, the phase speed accelerates slowly, over a distance a little more than $5 \mu\text{m}$, while the deceleration occurs faster, over a distance of $3 \mu\text{m}$ until the curve in the chiral medium equals the curve in the achiral medium (reference), as shown in Fig. 3(b).

To find the phase acceleration (or 1-D phase gradient in z in this case, since the propagation speed is constant, this phase gradient is proportional to the phase acceleration) the derivative of (4) is taken with respect to z , then:

$$\frac{d\omega_{non}}{dz} = -k\nu_0 \frac{1}{Re(A)^2} \frac{dRe(A)}{dz} \quad (8)$$

It is assumed here that the strength of the non-canonical vortex is high. Physically, this suggests that the interaction of the beam with the chiral medium is strong and there is a significant topological deformation of the beam. Formally, this means that $\frac{1}{Re(A)^2}$ can be Taylor expanded and replacing the Taylor expansion in (8) up to the linear term in z we have:

$$\frac{d\omega_{non}}{dz} = -k\nu_0 \left(\frac{1}{Re(A)^2} \Big|_{z_0} - \frac{1}{Re(A)^3} \Big|_{z_0} \Delta z \right) \frac{dRe(A)}{dz} \quad (9)$$

Where z_0 is a point inside the region of interest. Since $Re(A)$ is high, the second term in the expansion can be ignored, leaving only the constant term. Equation (9) becomes:

$$\frac{d\omega_{non}}{dz} = -k\nu_0 \frac{1}{Re(A)^2} \Big|_{z_0} \frac{dRe(A)}{dz} \quad (10)$$

Then, it can be seen that for high deformation of the beam $-\frac{dRe(A)}{dz}$ is proportional to the phase acceleration. This is because, is associated to torques extrema. It was found in [23] that when a particle is placed inside a chiral medium and a LG beam was passed through it, the absolute value of torque exerted to a particle in ϕ direction was a maxima just after start of the acceleration and just before the end of the deceleration region. In the non-canonical optical vortex model proposed in this article, when $-\frac{dRe(A)}{dz}$ is a maxima near $z = 4.2 \mu\text{m}$ (i.e. phase acceleration is a maxima) the first absolute value of torque maxima occurs according to [23]. Also, when there is an inflection point near $z = 10 \mu\text{m}$ (i.e. the phase jerk is a maxima) the second extreme of torque occurs according to Liu et al.

From the non-canonical optical vortex model, it can be concluded that the nature of each extreme torque is different. The first maxima of the absolute value of torque is associated with a maxima of phase acceleration and the second maxima is associated with a maxima of phase jerk (its derivative). This allows us to speculate that extrema in the torques may not only be related to phase acceleration, but also to its derivatives. Further, qualitatively the depth/strength of the extrema may be related to the order of the derivative with respect to z starting from the phase acceleration or in turn the quantity $-\frac{dRe(A)}{dz}$. This qualitative behavior that the non-canonical optical vortex model shows, may allow us to predict location and depth of torque extrema, only by analyzing the $-\frac{dRe(A)}{dz}$ and its derivatives.

Moreover, it was found via simulations that when increasing κ the real part of the free parameter $A_0(\lambda, \kappa)$ decreases, the phase acceleration starts before and more importantly the point where the phase start decelerating is shifted towards the left. This means that by knowing the exact analytical function of λ and κ one can construct the curve of the phase acceleration vs z for high amplitudes. This motivates future studies to construct and find this analytical function $A_0(\lambda, \kappa)$.

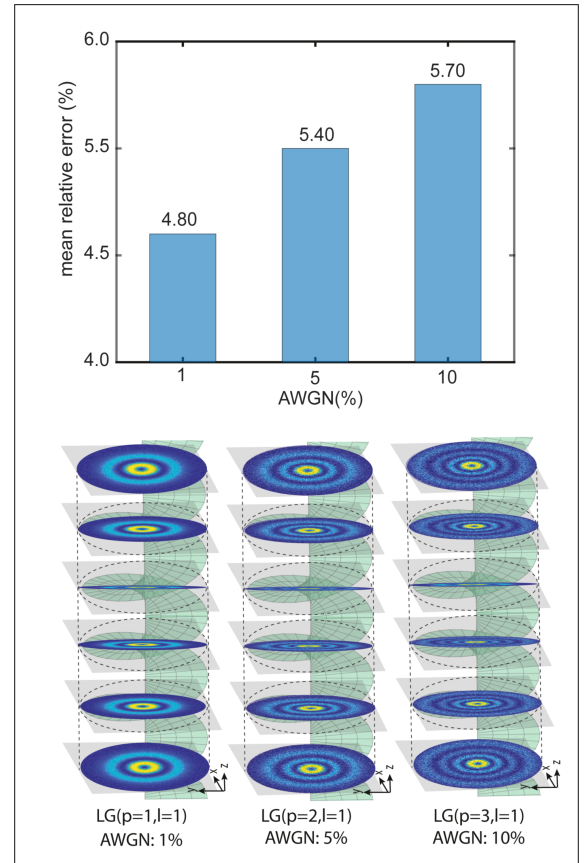


Fig. 4. Mean relative error of different LG modes with different percentage of AWGN. The beam evolution is evaluated and depicted as it travels the chiral media for different modes.

In order to validate the results, different beam modes are used. It is relevant to mention that the value of l does not present a strong impact in the results, as there is evidence in the literature [28], [31] that higher values of l becomes unrealistic for a chiral environment. This is attributed to the fact that values of $|l|$ greater than the unit brings unstable vortices, leading to a rapid decay towards a single charge component [28], [31]. The value of l is therefore fixed at unity. However, different p values, and the incorporation of an Additive White Gaussian Noise (AWGN) [32], into the model present effects on the proposed approach leading to the mean relative error (calculated in the acceleration and deceleration region) presented in FIG. 4. Notice that the mean relative error does not exceed six percent, which brings confidence to the proposed approach.

The implications of the proposed approach involve many fields of science and engineering. For instance, in the biological imaging and microscopy field the use of Laguerre–Gaussian beams in chiral media can improve the resolution and imaging capabilities of optical systems in biological microscopy. The enhanced phase control can lead to better imaging of biological samples, including cells, tissues, and even subcellular structures. This could facilitate advances in understanding cellular processes and studying complex biological systems at a higher resolution [33]. Concerning the optical manipulation in biological studies, the ability to control the phase distribution of

Laguerre–Gaussian beams in a chiral medium can enable a more precise and comprehensive manipulation (via torque or force) of biological objects (e.g., single cells and nanoparticles) [34], [35]. Focusing on the optical communication and information processing, the phase manipulation of Laguerre–Gaussian beams enables a robust control of the topological charge and distinguishability property, which may enhance the capacity and robustness of optical communication systems, leading to more efficient data transmission and secure communication protocols [36], [37]. Finally, there could be implications for quantum information processing and quantum optics [38]. The use of Laguerre–Gaussian beams in chiral media might play a role in quantum communication, quantum cryptography, and quantum entanglement-based applications through the transformation of a single l to a superposition of various modes [39].

III. CONCLUSION

To conclude, the distinguishability property of phase speed of a Laguerre Gaussian beam is hinted via topological transformation of a canonical vortex into a non-canonical vortex in chiral medium. This suggests that phase speed dependence on A , could be reduced for a non-interacting LG beam using the simplest function, which for a canonical vortex is $\omega \propto 1/l$. Furthermore, as shown in Figs. 2(b) and 3, the real part of the non-canonical strength is closely related to what regions the phase speed of a vortex beam accelerates and decelerates in a chiral medium. From the graph $Re(A)$ vs z the slope sign of this curve indicates if the phase speed accelerates (negative slope) or decelerates (positive slope), and the steeper of this slope dictates how fast is this acceleration/deceleration.

More importantly, the same physical scenario discussed in this article can be explained by using quantum mechanics [29]. The resulting elliptical beam after passing through a slab of chiral medium, is in a superposition of different LG modes with different values of the topological charge l (an analogous phenomenon occurs in [29]). Now, global averages of observable (i.e. over the whole beam), like angular momentum, do not change $\langle L \rangle = lh$, but there is a redistribution of the local angular momentum density and given that the topological charge locally can take different values, quantum mechanically local averages of observables do change with z . This is what is observed in [23] for the phase speed, where there is phase acceleration and deceleration in some regions, and here is attributed to the local variation in l modes. Incidentally, this suggests that the local average of the phase speed does depend on l , and therefore, there exists a distinguishability property in the local average of the phase speed.

REFERENCES

- [1] L. Gong et al., “Optical orbital-angular-momentum-multiplexed data transmission under high scattering,” *Light: Sci. Appl.*, vol. 8, 2019, Art. no. 27.
- [2] D. Lee, H. Sasaki, H. Fukumoto, K. Hiraga, and T. Nakagawa, “Orbital angular momentum (OAM) multiplexing: An enabler of a new era of wireless communications,” *IEICE Trans. Commun.*, vol. 100, no. 7, pp. 1044–1063, 2017.
- [3] X. Chen, W. Xue, H. Shi, J. Yi, and W. E. Sha, “Orbital angular momentum multiplexing in highly reverberant environments,” *IEEE Microw. Wireless Compon. Lett.*, vol. 30, no. 1, pp. 112–115, Jan. 2020.
- [4] H. Zhao, B. Quan, X. Wang, C. Gu, J. Li, and Y. Zhang, “Demonstration of orbital angular momentum multiplexing and demultiplexing based on a metasurface in the terahertz band,” *ACS Photon.*, vol. 5, no. 5, pp. 1726–1732, 2018.
- [5] Y. Chen, S. Liu, Y. Lou, and J. Jing, “Orbital angular momentum multiplexed quantum dense coding,” *Phys. Rev. Lett.*, vol. 127, no. 9, pp. 093601–093607, 2021.
- [6] G. Gibson et al., “Free-space information transfer using light beams carrying orbital angular momentum,” *Opt. Exp.*, vol. 12, no. 22, pp. 5448–5456, 2004.
- [7] S. Li and J. Wang, “Experimental demonstration of optical interconnects exploiting orbital angular momentum array,” *Opt. Exp.*, vol. 25, no. 18, pp. 21537–21547, 2017.
- [8] S. Fu, Y. Zhai, C. Yin, H. Zhou, and C. Gao, “Mixed orbital angular momentum amplitude shift keying through a single hologram,” *OSA Continuum*, vol. 1, no. 2, pp. 295–308, 2018.
- [9] J. H. Jeong and J.-M. Jeong, “Binary amplitude shift keying based signal processing for Brillouin optical correlation domain analysis,” *J. Korean Phys. Soc.*, vol. 61, pp. 1975–1980, 2012.
- [10] C. Heinisch, S. Lichtenberg, V. Petrov, J. Petter, and T. Tschudi, “Phase-shift keying of an optical Bragg cell filter,” *Opt. Commun.*, vol. 253, no. 4, pp. 320–331, 2005.
- [11] Z. Li, J. Su, and X. Zhao, “Two-step system for image receiving in OAM-SK-FSO link,” *Opt. Exp.*, vol. 28, no. 21, 2020, Art. no. 30520.
- [12] K. Liu, Y. Cheng, Y. Gao, X. Li, Y. Qin, and H. Wang, “Super-resolution radar imaging based on experimental oam beams,” *Appl. Phys. Lett.*, vol. 110, 2017, Art. no. 164102.
- [13] S. Sato, M. Ishigure, and H. Inaba, “Optical trapping and rotational manipulation of microscopic particles and biological cells using higher-order mode ND:YAG laser beams,” *Electron. Lett.*, vol. 27, no. 20, pp. 1831–1832, 1991.
- [14] J. A. Grieve et al., “Hands-on with optical tweezers: A multitouch interface for holographic optical trapping,” *Opt. Exp.*, vol. 17, no. 5, 2009, Art. no. 3595.
- [15] A. Arias et al., “Simultaneous rotation, orientation and displacement control of birefringent microparticles in holographic optical tweezers,” *Opt. Exp.*, vol. 21, no. 1, pp. 102–111, 2013.
- [16] A. Bianchetti, P. Etchepareborda, and A. Federico, “Determining the fractional topological charge shifting in perfect vortices from laser speckle,” *Opt. Commun.*, vol. 441, pp. 74–79, 2019.
- [17] M. Liu, “Measuring the fractional and integral topological charges of the optical vortex beams using a diffraction grating,” *Optik*, vol. 126, no. 24, pp. 5263–5268, 2015.
- [18] J. Zhu et al., “Probing the fractional topological charge of a vortex light beam by using dynamic angular double slits,” *Photon. Res.*, vol. 4, no. 5, pp. 187–190, 2016.
- [19] L. Allen, M. W. Beijersbergen, R. J. Spreeuw, and J. P. Woerdman, “Orbital angular momentum of light and the transformation of Laguerre–Gaussian laser modes,” *Phys. Rev. A*, vol. 45, no. 11, 1992, Art. no. 8185.
- [20] A. Pazmino, P. Iza, M. Alvarez-Alvarado, and E. Lamilla, “Helical-phase distinguishability for the phase distribution of Laguerre–Gaussian beams,” 2023, *arXiv:2302.05495*.
- [21] A. T. O’Neil, I. MacVicar, L. Allen, and M. J. Padgett, “Intrinsic and extrinsic nature of the orbital angular momentum of a light beam,” *Phys. Rev. Lett.*, vol. 88, no. 5, 2002, Art. no. 4.
- [22] N. B. Simpson, K. Dholakia, L. Allen, and M. J. Padgett, “Mechanical equivalence of spin and orbital angular momentum of light: An optical spinner,” *Opt. Lett.*, vol. 22, no. 1, pp. 52–54, 1997.
- [23] X. Liu, J. Li, Q. Zhang, G. Pang, and D. J. Gelmecha, “Revolution and spin of a particle induced by an orbital-angular-momentum-carrying Laguerre–Gaussian beam in a dielectric chiral medium,” *Phys. Rev. A*, vol. 98, no. 5, pp. 1–6, 2018.
- [24] N. B. Simpson, L. Allen, and M. J. Padgett, “Optical tweezers and optical spanners with Laguerre–Gaussian modes,” *J. Modern Opt.*, vol. 43, no. 12, pp. 2485–2492, 1996.
- [25] A. Lakhtakia, V. V. Varadan, and V. K. Varadan, “Field equations, Huygens’s principle, integral equations, and theorems for radiation and scattering of electromagnetic waves in isotropic chiral media,” *J. Opt. Soc. Am A*, vol. 5, no. 2, pp. 175–184, Feb. 1988. [Online]. Available: <https://opg.optica.org/josaa/abstract.cfm?URI=josaa-5-2-175>
- [26] E. Plum, V. A. Fedotov, and N. I. Zheludev, “Specular optical activity of achiral metasurfaces,” *Appl. Phys. Lett.*, vol. 108, 2016, Art. no. 141905.

- [27] G. D. Fasman, *Circular Dichroism and the Conformational Analysis of Biomolecules*, 1st ed. Berlin, Germany: Springer, 2013.
- [28] G. Molina-Terriza, E. M. Wright, and L. Torner, "Propagation and control of noncanonical optical vortices," *Opt. Lett.*, vol. 26, no. 3, pp. 163–165, 2001.
- [29] G. Molina-Terriza, J. Recolons, J. P. Torres, L. Torner, and E. M. Wright, "Observation of the dynamical inversion of the topological charge of an optical vortex," *Phys. Rev. Lett.*, vol. 87, no. 2, 2001, Art. no. 23902.
- [30] T. Fadeyeva, C. N. Alexeyev, B. Sokolenko, M. Kudryavtseva, and A. Volyar, "Non-canonical propagation of high-order elliptic vortex beams in a uniaxially anisotropic medium," *Ukrainian J. Phys. Opt.*, vol. 12, no. 2, pp. 62–82, 2011.
- [31] A. A. Voitiv, J. M. Andersen, P. C. Ford, M. T. Lusk, and M. E. Siemens, "Hydrodynamics explanation for the splitting of higher-charge optical vortices," *Opt. Lett.*, vol. 47, no. 6, pp. 1391–1394, Mar. 2022. [Online]. Available: <https://opg.optica.org/ol/abstract.cfm?URI=ol-47-6-1391>
- [32] B. Hughes, "On the error probability of signals in additive white Gaussian noise," *IEEE Trans. Inf. Theory*, vol. 37, no. 1, pp. 151–155, Jan. 1991.
- [33] L. Chen, J. Lei, and J. Romero, "Quantum digital spiral imaging," *Light: Sci. Appl.*, vol. 3, no. 3, 2014, Art. no. e153.
- [34] L. Gong, B. Gu, G. Rui, Y. Cui, Z. Zhu, and Q. Zhan, "Optical forces of focused femtosecond laser pulses on nonlinear optical Rayleigh particles," *Photon. Res.*, vol. 6, no. 2, pp. 138–143, Feb. 2018. [Online]. Available: <https://opg.optica.org/prj/abstract.cfm?URI=prj-000000000006-2-138>
- [35] M. Padgett and R. Bowman, "Tweezers with a twist," *Nature Photon.*, vol. 5, no. 6, pp. 343–348, 2011.
- [36] E. Lamilla, C. Sacarelo, M. S. Alvarez-Alvarado, A. Pazmino, and P. Iza, "Optical encoding model based on orbital angular momentum powered by machine learning," *Sensors*, vol. 23, no. 5, 2023, Art. no. 2755. [Online]. Available: <https://www.mdpi.com/1424-8220/23/5/2755>
- [37] A. E. Willner et al., "Optical communications using orbital angular momentum beams," *Adv. Opt. Photon.*, vol. 7, no. 1, pp. 66–106, Mar. 2015. [Online]. Available: <https://opg.optica.org/aop/abstract.cfm?URI=aop-7-1-66>
- [38] T. Stav et al., "Quantum entanglement of the spin and orbital angular momentum of photons using metamaterials," *Science*, vol. 361, no. 6407, pp. 1101–1104, 2018, doi: [10.1126/science.aat9042](https://doi.org/10.1126/science.aat9042).
- [39] B. Ndagano, I. Nape, M. A. Cox, C. Rosales-Guzman, and A. Forbes, "Creation and detection of vector vortex modes for classical and quantum communication," *J. Lightw. Technol.*, vol. 36, no. 2, pp. 292–301, Jan. 2018. [Online]. Available: <https://opg.optica.org/jlt/abstract.cfm?URI=jlt-36-2-292>